Article

Removal of Tetracycline Hydrochloride from Water by Visible-Light Photocatalysis Using BiFeO$_3$/BC Materials

Zhengyang Fang [1,2], Honghui Jiang [1], Jiamin Gong [1], Hengrui Zhang [1], Xi Hu [1], Ke Ouyang [1], Yuan Guo [3], Xinjiang Hu [1], Hui Wang [1,4,*] and Ping Wang [1,*]

[1] College of Environmental Science and Engineering, Central South University of Forestry and Technology, Changsha 410004, China
[2] Guangzhou Institute of Geochemistry, Chinese Academy of Sciences, Guangzhou 510640, China
[3] Institute of Bast Fiber Crops, Chinese Academy of Agricultural Sciences, Changsha 410205, China
[4] Faculty of Life Science and Technology, Central South University of Forestry and Technology, Changsha 410004, China
* Correspondence: wanghui@csuft.edu.cn (H.W.); csfuwp@163.com (P.W.)

Abstract: It is widely considered that photocatalysis is an effective and eco-friendly method of dealing with organic pollutants dissolved in water. Nonetheless, photocatalysts still have some drawbacks, such as poor visible-light absorption, easy recombination of photogenerated charge carriers, and limited active sites. In this study, bismuth ferrite coupled with biochar material (BiFeO$_3$/BC) was simply synthesized, and its photocatalysis reactivity was systemically examined under an irradiation of $\lambda > 400$ nm. The experimental results showed that under a relatively acidic environment, the removal rate of tetracycline hydrochloride reached 95%. Using a variety of characterization investigations, we analyzed the morphology structure and chemical composition of BiFeO$_3$/BC. In consideration of simple preparation and high respondence toward visible light, further explorations of BiFeO$_3$/BC and its properties and optimized degradation conditions are worthwhile.

1. Introduction

As an effective antibiotic, tetracycline hydrochloride (TCH) is widely used in China [1]. It has the beneficial effect of disinfecting bacteria, and is therefore applied in producing feeds for livestock and poultry [2]. As a result, wastewater discharged from farms inevitably contains TCH. However, presently applied technologies cannot completely remove this kind of antibiotic. When TCH accumulates in a natural environment, resistance gradually develops in the bacteria. Once these antibiotic-resistant genes (ARGs) are transferred into pathogens, they can pose a threat to human health [3–5]. Therefore, the development of a high-performance and eco-friendly method to eliminate TCH in the environment is imperative.

Photocatalysis has been proven to be an effective method for degrading antibiotics [6–8]. When a photocatalyst is activated by a specific wavelength of irradiation, photo-induced electron pairs are produced on the surface of the catalyst. The pollutant then undergoes a redox reaction and is eventually removed from the solution. However, according to a recent report, the widely applied photocatalyst TiO$_2$ (P25) needs UV light to be activated; nevertheless, the efficiency of degradation still requires improvement [9]. In another study, doped g-C$_3$N$_4$ was used for visible-light-conducted degradation; however, it requires a relatively long illumination time to remove most of the TCH [10]. In the pursuit of high-speed degradation, ZnO/TiO$_2$ NBT was synthesized; however, the preparation procedure for ZnO/TiO$_2$ NBT is complicated [11]. For the purpose of solving the problems mentioned above, we chose BiFeO$_3$ as a photocatalyst to achieve both relatively rapid degradation and

simple preparation. $BiFeO_3$ has a relatively narrow band gap and responds to visible light. It has been used to deal with organic dyes and pharmaceutical residues such as methylene blue, cefixime, and ciprofloxacin [12–18]. Few past researchers have studied the photodegradation mechanism of TCH by $BiFeO_3$. In general, some organic intermediates of smaller molecules were produced during the degradation of TCH, while TOC decreased [19,20].

Carbon-based materials have been shown to be helpful in removing common contaminants in water, such as heavy metal ions and organic acids. Using waste biomass or other natural materials to remove pollutants from water has proven to be a cost-effective method [21–23]. Among them is biochar, which is made through the pyrolysis of animal or plant biomass. A variety of agricultural waste, such as Eichhornia crassipes and Eucalyptus sawdust, can be used to produce biochar [24–26]. In China, kenaf is widely planted; it is feasible to recycle kenaf waste to achieve environment-friendly material production. Multiple reports have stated that the pyrolysis yields of kenaf fibers typically have the excellent properties of biochar [27–30], such as abundant carbon content, large specific surface area, and high adsorption capacity [31,32]. Moreover, biochar has the ideal optical property of absorbing visible light [33,34]. As a result, compositing biochar with $BiFeO_3$ may improve photocatalytic efficiency [35–38].

To provide a new method for TCH degradation, we prepared a new bismuth ferrite coupled with biochar material ($BiFeO_3$/BC). The characteristics of the synthesized material were analyzed, and the photodegradation properties of $BiFeO_3$/BC toward TCH under visible-light irradiation were systemically studied. Photocatalytic optimal reacting conditions were investigated by varying pH level, $BiFeO_3$/BC dosage, and initial TCH concentration. Some further considerations regarding the transparency and influences of inorganic ions are also discussed in this paper. The methodology introduced in this study can provide another prospective method for the photocatalytic treatment of pharmaceutical wastewater.

2. Results and Discussions

2.1. Characterization

The morphology and structure of uncoupled biochar (BC), $BiFeO_3$, and $BiFeO_3$/BC were analyzed using scanning electron microscopy (SEM). As shown in Figure 1a, BC presents lamellar structure, which increases the specific surface area of the material. $BiFeO_3$ (Figure 1b) presents an irregular agglomeration in a crystalline shape [39], which is helpful in binding together slack biochar, although the photocatalytic ability of the interior crystal would probably be restrained [5]. As presented in Figure 1c,d, $BiFeO_3$/BC was compactly synthesized; pore structures and rod-like clusters can be observed [25], which expands the reaction area. This structure may enable $BiFeO_3$/BC to reach higher photocatalytic performance. Figure S1 exhibits the N_2 adsorption–desorption isotherms and the results of pore size distribution of the $BiFeO_3$/BC. The measured specific surface area of the $BiFeO_3$/BC was 26.739 m^2/g.

The FT-IR spectra of $BiFeO_3$/BC, $BiFeO_3$, and BC are shown in Figure 2. In the absorption curve of $BiFeO_3$/BC and $BiFeO_3$, there is a sharp peak near 550 cm^{-1}, which may be caused by the vibration of the octahedral structure of bismuth [39]. BC, however, has no obvious absorption peak at this wave number. The vibration band at 835 cm^{-1} represents a potential occurrence of a tri-s-triazine ring appearing in organic pyrolysis products [40]. The common vibration bands at nearly 1060 and 1110 cm^{-1} suggest the potential existence of ν(C–O) [41]. $BiFeO_3$/BC exhibits another peak at 1350 cm^{-1}, suggesting that the material contains a C–C bond; it may also contain a C–N bond due to the nitrogen environment in the heating process. All three materials had peaks at wave numbers of about 1620 and 3400 cm^{-1}, which indicate the presence of H–O–H bending vibration and hydroxyl (–OH) groups, respectively [42–45]. In summary, $BiFeO_3$/BC effectively retained the properties of typical biochar and $BiFeO_3$.
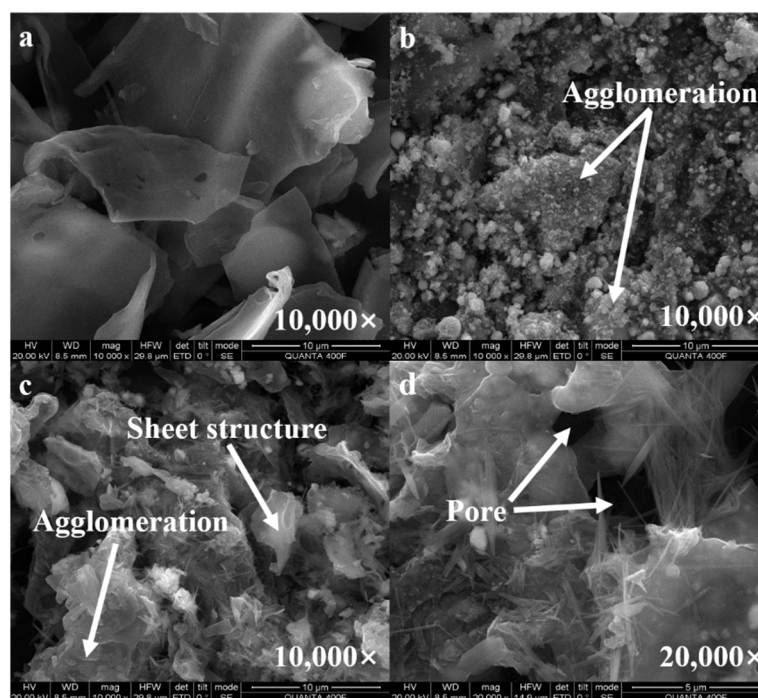
Figure 1. (**a**) SEM images of uncoupled biochar (BC), (**b**) bismuth ferrite (BiFeO$_3$), and (**c**,**d**) bismuth ferrite coupled with biochar material (BiFeO$_3$/BC).
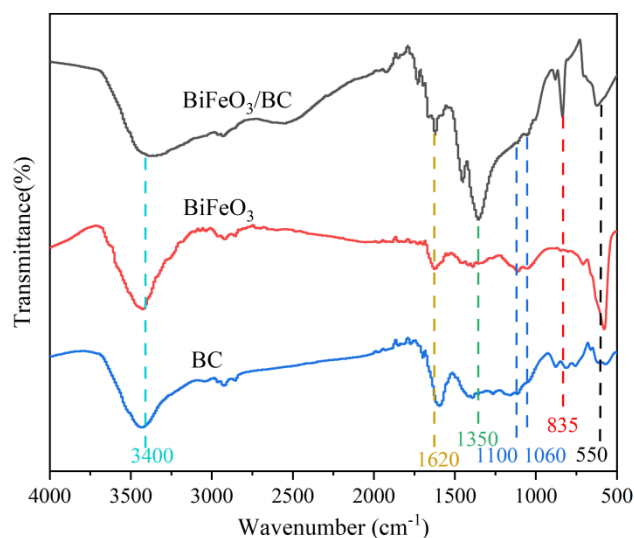

Figure 2. FT-IR spectroscopy of BC, BiFeO$_3$/BC, and BiFeO$_3$.

To determine the interaction between BiFeO$_3$ and the other components in BiFeO$_3$/BC, the composites were characterized by XPS (Figure 3) and XRD (Figure S2).

Figure 3 displays the XPS spectra of the survey, Bi 4f, C 1s, and O 1s. Bi4f$_{5/2}$, and Bi4f$_{7/2}$ wave peaks of the bismuth element (Figure 3b), which are symmetrical at 163.8 and 158.4 eV. This indicates the presence of BiFeO$_3$ in the material. Also shown in the XRD results (see Figure S2) are several similar absorption peaks between BiFeO$_3$/BC and pure BiFeO$_3$, indicating that BiFeO$_3$/BC has characteristics analogous to those of pure BiFeO$_3$. Among them, (003), (021), and (300) represent the single-phase perovskite structure of BiFeO$_3$, which proves that the BiFeO$_3$ was successfully synthesized using our method. Interestingly, we observed the (201) and (002) signals of Bi$_2$Fe$_4$O$_9$, and (311) and (440) signals of Fe$_2$O$_3$ as well [25,37,46,47]. To the best of our knowledge, although Bi$_2$Fe$_4$O$_9$ and Fe$_2$O$_3$ seem to be impurities as for BiFeO$_3$, they are also extensively studied photocatalysts. Interactions

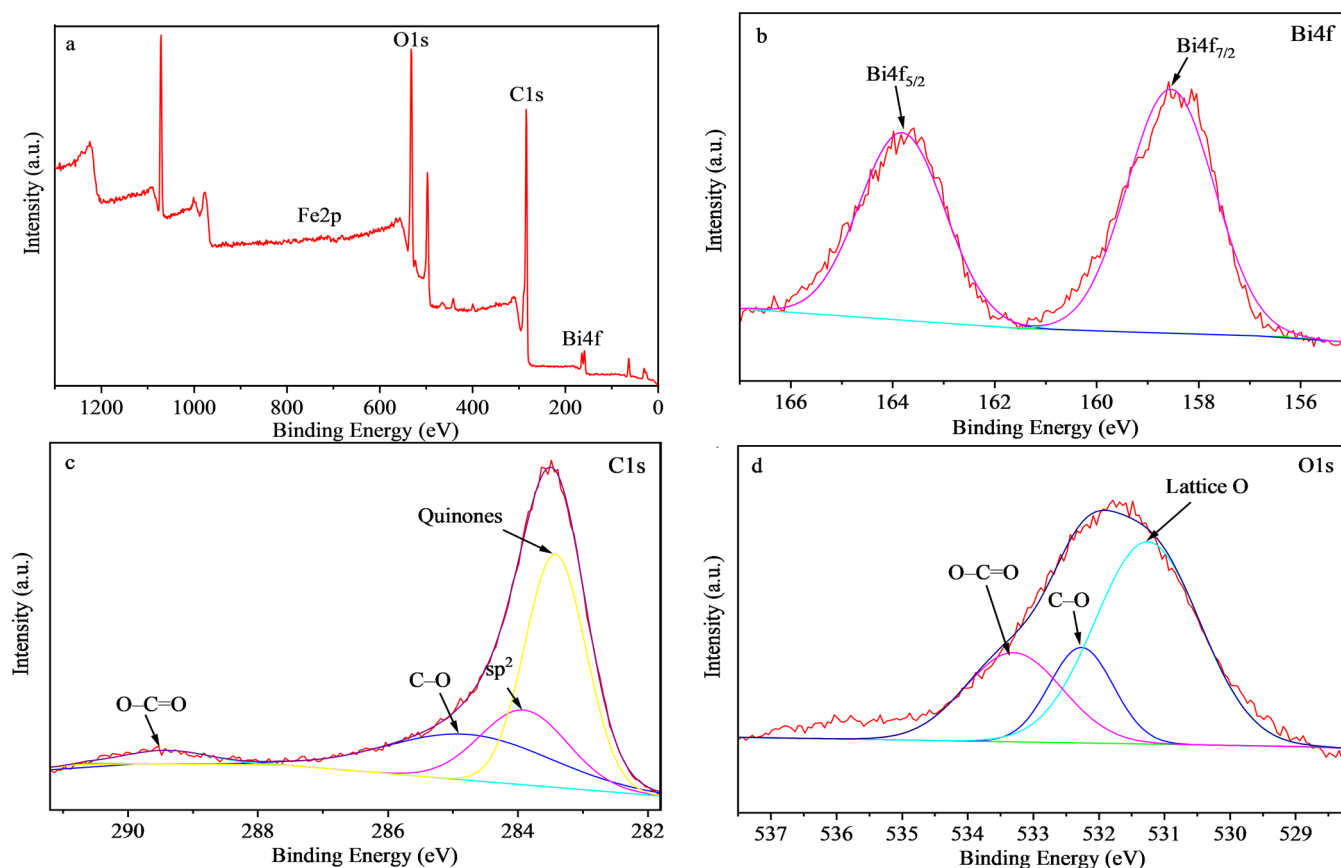between several active materials and mechanisms of coworking degradation may therefore require further study.

Figure 3. XPS spectra of BiFeO$_3$/BC (**a**) survey, (**b**) Bi 4f, (**c**) C 1s, and (**d**) O 1s.

As seen in Figure 3c, a small wave peak exists at 289 eV for the carbon element, indicating the existence of an O–C=O bond in the material [48]. Next, the signal at 285 eV was assigned to the C–O bond, which agreed with the FT-IR analysis [49,50]. In addition, a large peak at 284 eV corresponds to sp^2 hybrid carbon [47], suggesting the possibility of graphite or graphene in the material. The peak at 283.4 eV, which indicates the existence of quinones, seems to be the strongest peak; a similar result was reported in the literature [51]. Quinones were confirmed to facilitate photodegradation processes by promoting the generation of $^1O_2$ and OH• under irradiation [52]. The characteristic peak of the oxygen (Figure 3d) element is relatively wide, and the wave peak at 533.5 eV suggests the presence of an O–C=O bond. The presence of a peak at 532.3 eV further confirms that BiFeO$_3$/BC includes C–O bonds [26,39]. Finally, the presence of a peak at 531.2 eV indicates a lattice oxygen species [13]. Notably, the combination of lattice oxygen and H$_2$O can facilitate photocatalysis degradation progress, as they are precursors to free radicals [44]. These results demonstrate that the BiFeO$_3$/BC composites were properly prepared.

The optical properties of BiFeO$_3$/BC were analyzed using UV–Vis diffuse reflectance spectroscopy (Figure 4a). The sample was observed to have an effective absorption capacity for visible light. In comparison with previous studies, we determined that the red-shift phenomenon due to binding to the BC improves the overall absorption properties of BiFeO$_3$/BC for visible light [36,53,54]. After λ = 450 nm, a slight decrease in the absorption of light by BiFeO$_3$/BC was found, while no such decrease was observed for the BC substrate material. The reason for this phenomenon may be the perovskite structure of BiFeO$_3$. Typically, a significant decrease in absorption can be observed at around 550 nm [17,19,48]. Combined with the SEM results, we think that the combination of BC with BiFeO$_3$ achieves efficient absorption of visible light by changing the overall morphology of the material.
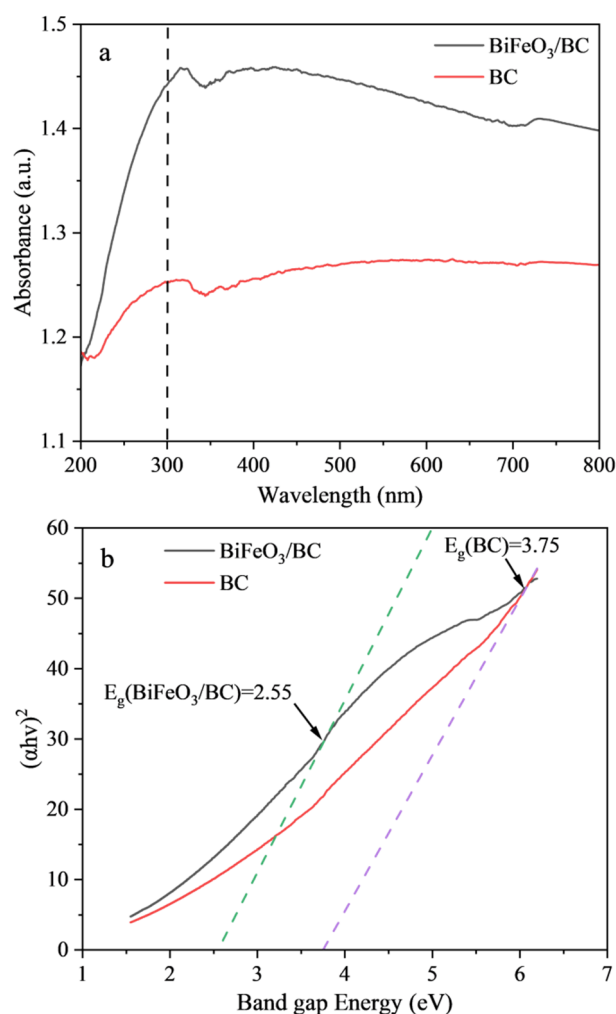
Figure 4. (**a**) UV–Vis spectra of $BiFeO_3/BC$ and BC; (**b**) $(\alpha hv)^2$ versus hv plot of $BiFeO_3/BC$ and BC.

The optical band energy (E_g) of $BiFeO_3/BC$ and BC was measured using Tauc's method (Equation (1)).

$$(\alpha hv)^n = A(hv - E_g) \tag{1}$$

where α represents the absorption coefficient; h is the Planck constant; v is the photon frequency; n is determined by the type of optical transition, where the value of n for the direct bandgap semiconductor $BiFeO_3$ is 2; A is a constant; and E_g represents a band gap, which can be obtained by extrapolating the linear part of the graph to $(\alpha hv)^2 = 0$ [17,36]. The estimated band gaps of $BiFeO_3/BC$ and BC were 2.55 eV and 3.75 eV, respectively, as shown in Figure 4b. The combination with $BiFeO_3$ substantially reduces the band gap of BC and facilitates the overall response of the material to visible light.

2.2. Experimental Section

2.2.1. Effect of pH on Photocatalytic Efficiency

Figure S3 excludes the effect of the photolysis process of TCH itself; even after 3 h of self-degradation, only 6% of TCH was removed from the solution.

Generally, the adsorption of pollutants on catalysts can promote photodegradation efficiency. The adsorption performance was tested to confirm the adsorption capacity of $BiFeO_3/BC$ and the contribution rate of TCH removal by adsorption and photocatalysis. The experimental results are shown in Figure S4. Within 60 min, the adsorption process could remove 10~30% of TCH in the water, indicating that the material has a certain adsorption capacity for TCH, which provides the prerequisite for photocatalytic degradation

on the material surface. To explore the anti-interference ability of BiFeO$_3$/BC in a complex, practical environment, and to determine the possible influence of BC on photocatalytic performance, we conducted photocatalytic experiments under highly acidic, acidic, neutral, and alkaline conditions.

As shown in Figure 5a, the degradation rate reached more than 70% after 90 min of reaction, except in cases where pH = 7. The degradation rate remained insignificantly high at pH = 4 after irradiation started. As seen in Figure 5b, the BC exhibited almost no photocatalytic activity. This result is consistent with that in a previous report [19]. Combined with the results of the zeta potential analysis (see Figure S5 for more details), it was expected that when the pH turned alkaline, the degradation ratio would further decrease because both the BiFeO$_3$/BC and TCH were negatively charged [19,55]. Instead, the results indicated that BiFeO$_3$/BC could maintain much the same degradation efficiency as under acidic environments. Drawing on another similar study, we speculated that inorganic ions affected the degradation process, especially under neutral conditions; the solution contained a certain amount of NaCl attributed to NaOH and HCl used to adjust the pH, which may restrain the degradation process [19].
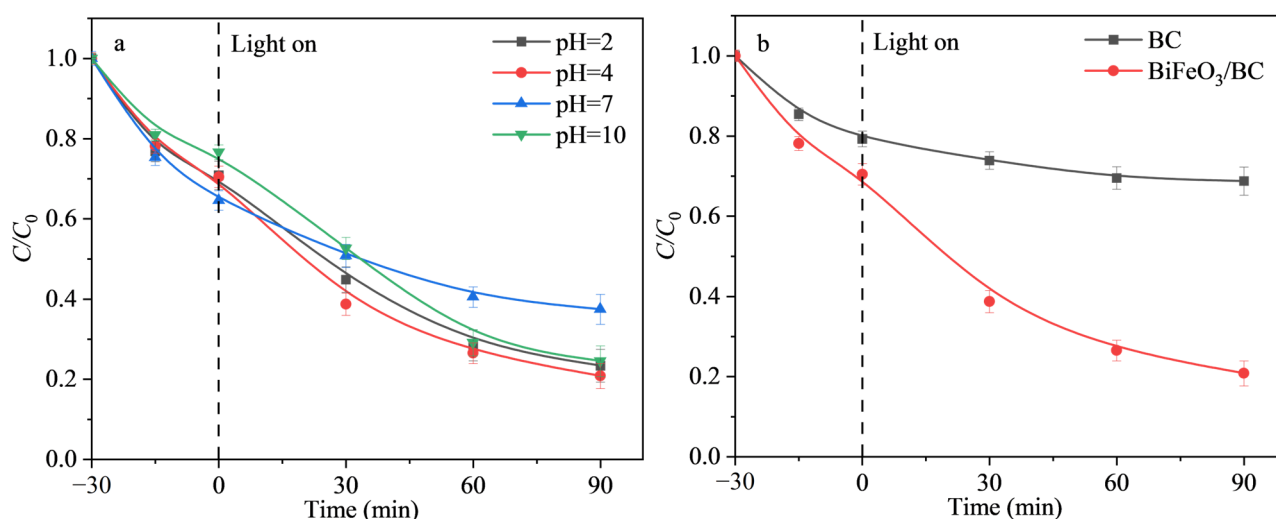

Figure 5. (**a**) Effect of pH on photocatalytic efficiency. (**b**) Comparison of photocatalytic degradation capacity of BC and BiFeO$_3$/BC at pH = 4 (3 replicates; dosage of BiFeO$_3$/BC or BC = 0.5 g; $C_{0\,(TCH)}$ = 30 mg/L).

2.2.2. Effect of Photocatalysis Dosage

To elucidate the influence of different additions of BiFeO$_3$/BC on photocatalytic capacity, and to find the best quantity or the most appropriate range, investigations using different photocatalyst dosages were carried out in this study. Figure 6 shows the comparison of efficiency under the conditions of different BiFeO$_3$/BC dosages.

It was determined that the optimal dosage of BiFeO$_3$/BC was 0.05 g and that the removal rate was up to 89%. In the range of 0.03~0.1 g, the removal rate could be kept above 80%. Compared with Figure 5, where the initial concentration and catalyst quantity simultaneously reduced, the enhancement in photocatalytic efficiency could be observed. It was also found that the addition of BiFeO$_3$/BC could change the physical properties of the mixture. In the case of a lower dosage, there were fewer catalyst particles in the solution, which may be more favorable for the transmission of light to the bottom of the container, thus improving the efficiency of the degradation.
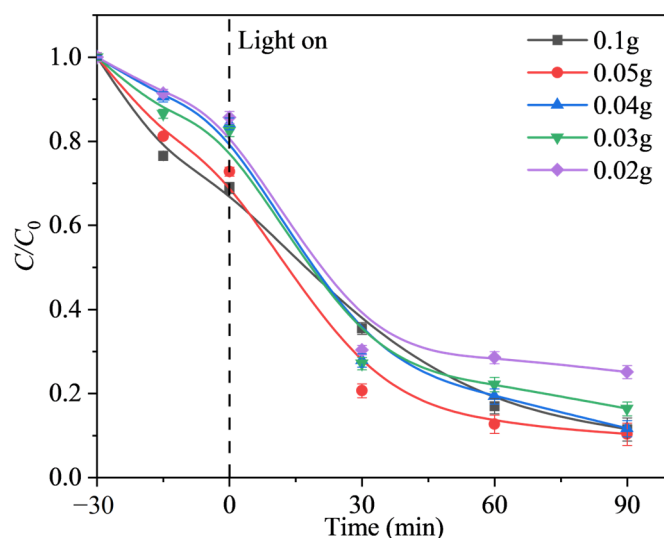
Figure 6. Effect of dosage on photocatalytic efficiency (3 replicates; pH = 4; $C_{0(TCH)}$ = 10 mg/L).

2.2.3. Effect of Initial TCH Concentration

To determine the suitable initial concentrations of TCH, we carried out experiments under different initial concentrations. Figure 7a exhibits the experimental results of photocatalysis reaction with initial concentrations of 5–30 mg/L of TCH. The degradation reaction kinetics were compared using the pseudo-first-order kinetics model (Figure 7b).
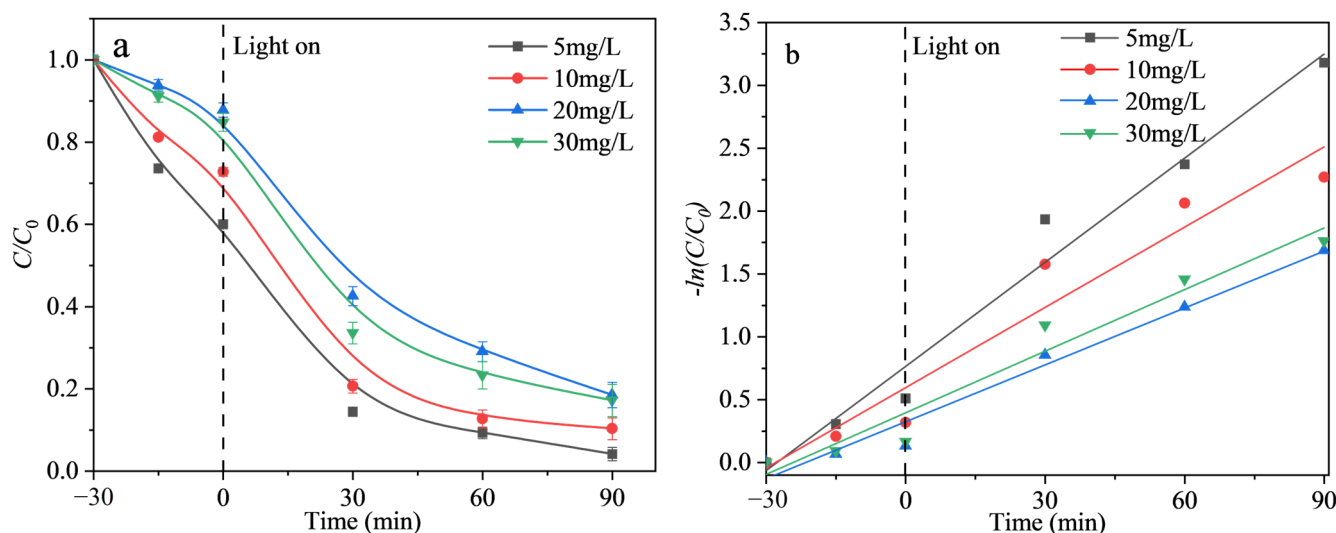

Figure 7. Effect of initial TCH concentrations on photocatalytic efficiency (**a**) and degradation reaction kinetics (**b**) (3 replicates; dosage of $BiFeO_3/BC$ = 0.05 g; pH = 4).

The calculated degradation rate constants (k) were 0.02761, 0.02128, 0.01508, and 0.01634 min^{-1}, for 5, 10, 20, and 30 mg/L initial concentration of TCH, respectively. $BiFeO_3/BC$ could achieve more than a 95% photocatalytic elimination rate when the initial concentration was 5 mg/L. Our experimental results showed that $BiFeO_3/BC$ is effective for the photocatalytic treatment of TCH under low concentrations (5–30 mg/L) and relatively acidic environments (pH = 4). Table 1 exhibits the degradation efficiencies under different experimental conditions as reported by several publications. These data indicate that $BiFeO_3/BC$ can achieve effective TCH degradation in a relatively short time in a mild environment. We neither applied UV light nor added H_2O_2 to the solution. In practical applications, this can avoid any possible secondary pollution caused by H_2O_2.

Table 1. TCH degradation efficiency comparison of different photocatalysts.

Photocatalyst	Initial Concentration (mg/L)	Photocatalyst Dosage	Degradation Rate; Time Duration	Note	Reference
Chitosan/TiO$_2$ (P25)	30–40	1.2 g/L	~95%; 360 min	UV	[9]
Bi$_5$O$_7$I/g-C$_3$N$_4$	20	1.0 g/L	~95%; 180 min		[10]
ZnO/TiO$_2$ NBT	10	0.2 g/L	100%; 20 min	Complexed material	[11]
BFO/BNQDs	10	0.2 g/L	88%; 120 min	H$_2$O$_2$ (10 mM)	[19]
BiFeO$_3$	40	2.0 g/L	100%; 150 min	UV, H$_2$O$_2$ (9.8 mM)	[20]
Bi$_2$WO$_6$/BiFeO$_3$/g-C$_3$N$_4$	10	0.1 g/L	83.68%; 45 min	H$_2$O$_2$ (8 M)	[55]
BiFeO$_3$/BC	10	0.02–0.12 g/L	88.32%; 90 min		This work

Previous studies have proved that during TCH degradation, some intermediates are simultaneously generated [11,20]. In this study, we found that the total carbon content (TC) and total inorganic carbon content (TIC) increased with photocatalysis processing, while the total organic carbon content (TOC) did not significantly change (see Figure S6). In combination with the above results, the concentration of TCH declined, so the degradation has been ongoing. However, the data pertaining to TOC were disturbed due to the organic carbon contained in BiFeO$_3$/BC. Therefore, we concluded that TCH was degraded, but complete mineralization was not achieved.

3. Materials and Methods

3.1. Materials and Chemicals

Kenaf (*Hibiscus cannabinus L.*) fiber was provided by the Institute of Bast Fiber Crops and Center of Southern Economic Crops, Chinese Academy of Agricultural Sciences (Beijing, China). Bismuth nitrate pentahydrate (Bi(NO$_3$)$_3$•5H$_2$O, AR grade) and ferric nitrate nonahydrate (Fe(NO$_3$)$_3$•9H$_2$O, AR grade) were purchased from Guangdong Guanghua Sci-Tech Co., Ltd. (Shantou, China). Tetracycline hydrochloride (C$_{22}$H$_{25}$ClN$_2$O$_8$, AR grade) was provided by Macklin Inc. (Shanghai, China). Ultrapure deionized water (H$_2$O) was used throughout this study.

3.2. Preparation of Bismuth Ferrite Coupled with Biochar Material (BiFeO$_3$/BC)

BC was prepared via the pyrolysis of kenaf stem. Kenaf stems were washed, dehydrated, and smashed into powder. The powder was then placed in a tube furnace for 30 min at a temperature of 600 °C with a nitrogen atmosphere. It was then cooled to room temperature for obtaining.

BiFeO$_3$/BC was prepared through the following procedure: The cleaned kenaf stem powder was pretreated with 0.1 M NaOH solution for 5 min at 85 °C. Then, 250 mL of 0.04 M Bi(NO$_3$)$_3$ and 250 mL of 0.04 M Fe(NO$_3$)$_3$ were added into the mixture, and the hybrid was stirred at 85 °C for 30 min. After dehydrating the mixture, the powder-like substance was pyrolyzed in a tube furnace for 30 min at a temperature of 600 °C in a nitrogen atmosphere. The cooled material was specified as BiFeO$_3$/BC. The pure BiFeO$_3$ was prepared using the sol-gel method. The mixture of Bi(NO$_3$)$_3$ and Fe(NO$_3$)$_3$ was dried to gelatinous matter and placed in a tube furnace, where the pyrolyzing time and temperature were the same as in the preparation of BiFeO$_3$/BC.

3.3. Characterization

Scanning electron microscopy (SEM) was carried out with a Quanta 400F thermal field emission scanning electron microscopy (FE-SEM; FEI, Hillsboro, OR, USA). The infrared spectroscopy was performed on a Nicolet 5700 Fourier transform infrared spectrometer (FT-IR; Thermo Nicolet Corporation, Waltham, MA, USA). The phase composition of

the material was analyzed by X-ray diffraction on a D8 Advance diffractometer with Cu Kα radiation (XRD; Bruker, Billerica, MA, USA). Chemical bonds and identities were analyzed on an ESCALAB 250XI X-ray photoelectron spectrometer (XPS; Thermo Fisher Scientific, Waltham, MA, USA). Zeta potential tests were performed with a Zetasizer Nano ZS zeta potential analyzer (Zeta potential, Malvern Panalytical, Malvern, UK). Ultraviolet–visible diffuse reflectance spectra of samples were analyzed with a UV-3600i plus UV–Vis spectrometer (UV-DRS, Shimadzu, Kyoto, Japan) at a wavelength range of 200–800 nm with $BaSO_4$ as the reference. The Brunauer–Emmett–Teller (BET) specific surface area and pore size of $BiFeO_3$/BC were measured with a 3 Flex analyzer (BET, Micromeritics Instruments, Norcross, GA, USA). Total organic carbon (TOC) in the photocatalysis process was measured with a TOC-V CPH analyzer (TOC, Shimadzu, Kyoto, Japan).

3.4. Photocatalytic Degradation of TCH

All experiments were carried out at 25 °C under magnetic stirring. A certain amount of $BiFeO_3$/BC (0.02~0.5 g) was added to a quartz reactor containing 250 mL of TCH (5~30 mg/L) solution. The pH conditions were adjusted with 0.01 M HCl and 0.01 M NaOH. Prior to the irradiation procedure, the solution was placed inside a black box without illumination for 30 min to reach equilibrium of adsorption–desorption. During the adsorption procedure, 5 mL samples were taken out every 15 min. All batch experiments were conducted in triplicate.

Photocatalysis assessments were carried out afterward with a 300 W xenon source (CEL-HXF300, Beijing China Education Au-light Co. Ltd., Beijing, China). A UV filter (λ > 400 nm) was placed above the quartz reactor, and the total illumination duration was 90 min. During the photocatalysis period, 5 mL samples were taken out every 30 min. All samples were filtered through a 0.22 μm polyether sulfone (PES) syringe filter. The concentrations of TCH residues were analyzed with a UV–Vis spectrophotometer (752N, Shanghai INESA Analytical Instrument Co., Ltd., Shanghai, China).

To assess potential impacts, a series of control experiments was designed. Adsorption tests were conducted by adding 0.5 g BC or $BiFeO_3$/BC in 30 mg/L TCH solution, with the same pH-altering procedure as in the adsorption tests. The mixture was then positioned without exposure to light for 6 h. A photolysis measurement was taken, 10 mg/L of TCH was irradiated, and the remaining concentration was examined after certain intervals. All analytical methods applied in the control tests were the same as those described in the photocatalysis experiments.

After determining the optimal conditions through batch experiments, a TOC experiment was conducted to evaluate the type of carbon content in the solution. The total inorganic carbon (TIC) was obtained through Equation (2):

$$TIC = TC - TOC \tag{2}$$

where *TC* represents total carbon, and *TOC* represents total organic carbon. The change in carbon content was assessed by calculating the concentration ratio (C/C_0) before and after the reaction.

4. Conclusions

In summary, novel $BiFeO_3$/BC photocatalysts were synthesized using a simple sol-gel method. The results of the characterization analysis showed that $BiFeO_3$/BC was successfully synthesized and has a good response in the visible light range. The results of the batch experiments showed that the material maintained good performance in a wide range of pH, and the degradation rate of TCH reached approximately 80% or higher in the range of pH 2–10. The presence of some inorganic ions and changes in the light transmission properties of the solution due to the amount of material added may have had an impact on photocatalytic efficiency. In contrast to other studies, our study demonstrates that $BiFeO_3$/BC enables the rapid degradation of TCH without additional UV light and

hydrogen peroxide. It is thought that $BiFeO_3/BC$ is a promising photocatalyst for the degradation of TCH by visible light.

Supplementary Materials: The following supporting information can be downloaded at: https://www.mdpi.com/article/10.3390/catal12111461/s1, Figure S1. (a) Plot of nitrogen adsorption–desorption isotherms and (b) pore size distribution curve of $BiFeO_3/BC$; Figure S2. XRD patterns of synthesized $BiFeO_3/BC$, synthesized $BiFeO_3$, and indications of Fe_2O_3, $BiFeO_3$, $Bi_2Fe_4O_9$; Figure S3. Photolysis curve of TCH (3 replicates; pH = 4; $C_{0(TCH)}$ = 10 mg/L); Figure S4. Experimental results of TCH adsorption using BC and $BiFeO_3/BC$ at different pH values (dosage of catalysts: 0.5 g; $C_{0(TCH)}$ = 30 mg/L); Figure S5. Zeta potential of $BiFeO_3/BC$ materials as a function of pH; Figure S6. TOC photocatalytic removal efficiencies of TCH (dosage of $BiFeO_3/BC$: 0.5 g; pH = 4; $C_{0(TCH)}$ = 10 mg/L); Figure S7. Comparison of the degradation efficiency of TCH after 90 min of reaction at different pH values. (3 replicates; dosage of $BiFeO_3/BC$: 0.5 g; $C_{0(TCH)}$ = 30 mg/L); Figure S8. Comparison of the degradation rate of TCH after 90 min of reaction at different dosing rates (3 replicates; pH = 4; $C_{0(TCH)}$ = 10 mg/L); Figure S9. Comparison of the degradation rate of TCH after 90 min of reaction at different initial concentrations. (3 replicates; dosage of $BiFeO_3/BC$ = 0.05 g; pH = 4). References [17,19,56–58] are cited in Supplementary Materials.

Author Contributions: Z.F.: investigation, methodology, writing—original draft., writing—review and editing. H.J.: writing—review and editing. J.G.: writing—review and editing. H.Z.: investigation. X.H. (Xi Hu): writing—review and editing. K.O.: writing—review and editing. Y.G.: writing—review and editing. X.H. (Xinjiang Hu): resources and writing—review and editing. H.W.: methodology, resources, writing—original draft, project administration, writing—review and editing. P.W.: funding acquisition, supervision, project administration. All authors have read and agreed to the published version of the manuscript.

Data Availability Statement: Data available on request from the authors.

Conflicts of Interest: The authors declare no conflict of interest.

References

1. Yu, Y.; Chen, L.; Fang, Y.; Jia, X.; Chen, J. High temperatures can effectively degrade residual tetracyclines in chicken manure through composting. *J. Hazard. Mater.* **2019**, *380*, 120862. [CrossRef] [PubMed]
2. Gu, B.J.; Zhang, X.L.; Bai, X.M.; Fu, B.J.; Chen, D.L. Four steps to food security for swelling cities. *Nature* **2019**, *566*, 31–33. [CrossRef] [PubMed]
3. Xu, R.; Yang, Z.H.; Wang, Q.P.; Bai, Y.; Liu, J.B.; Zheng, Y.; Zhang, Y.R.; Xiong, W.P.; Ahmad, K.; Fan, C.Z. Rapid startup of thermophilic anaerobic digester to remove tetracycline and sulfonamides resistance genes from sewage sludge. *Sci. Total Environ.* **2018**, *612*, 788–798. [CrossRef]
4. Granados-Chinchilla, F.; Rodríguez, C. Tetracyclines in Food and Feedingstuffs: From Regulation to Analytical Methods, Bacterial Resistance, and Environmental and Health Implications. *J. Anal. Methods Chem.* **2017**, *2017*, 1–24. [CrossRef]
5. Zhou, Y.; Liu, X.; Xiang, Y.; Wang, P.; Zhang, J.; Zhang, F.; Wei, J.; Luo, L.; Lei, M.; Tang, L. Modification of biochar derived from sawdust and its application in removal of tetracycline and copper from aqueous solution: Adsorption mechanism and modelling. *Bioresour. Technol.* **2017**, *245*, 266–273. [CrossRef]
6. Bagheri, S.; TermehYousefi, A.; Do, T.-O. Photocatalytic pathway toward degradation of environmental pharmaceutical pollutants: Structure, kinetics and mechanism approach. *Catal. Sci. Technol.* **2017**, *7*, 4548–4569. [CrossRef]
7. Wu, S.; Lin, Y.; Hu, Y.H. Strategies of tuning catalysts for efficient photodegradation of antibiotics in water environments: A review. *J. Mater. Chem. A* **2021**, *9*, 2592–2611. [CrossRef]
8. Xie, G.; Hu, X.; Du, Y.; Jin, Q.; Liu, Y.; Tang, C.; Hu, X.; Li, G.; Chen, Z.; Zhou, D.; et al. Light-driven breakdown of microcystin-LR in water: A critical review. *Chem. Eng. J.* **2021**, *417*, 129244. [CrossRef]
9. Ikhlef-Taguelmimt, T.; Hamiche, A.; Yahiaoui, I.; Bendellali, T.; Lebik-Elhadi, H.; Ait-Amar, H.; Aissani-Benissad, F. Tetracycline hydrochloride degradation by heterogeneous photocatalysis using TiO_2(P25) immobilized in biopolymer (chitosan) under UV irradiation. *Water Sci. Technol.* **2020**, *82*, 1570–1578. [CrossRef]
10. Yang, Y.; Lai, M.; Huang, J.; Li, J.; Gao, R.; Zhao, Z.; Song, H.; He, J.; Ma, Y. $Bi_5O_7I/g-C_3N_4$ Heterostructures with Enhanced Visible-Light Photocatalytic Performance for Degradation of Tetracycline Hydrochloride. *Front. Chem.* **2021**, *9*, 1107. [CrossRef]
11. Jiang, Q.; Han, Z.; Qian, Y.; Yuan, Y.; Ren, Y.; Wang, M.; Cheng, Z. Enhanced visible-light photocatalytic performance of ZIF-8-derived ZnO/TiO_2 nano-burst-tube by solvothermal system adjustment. *J. Water Process Eng.* **2022**, *47*, 102768. [CrossRef]

12. Iqbal, M.A.; Ali, S.I.; Amin, F.; Tariq, A.; Iqbal, M.Z.; Rizwan, S. La- and Mn-Codoped Bismuth Ferrite/Ti$_3$C$_2$ MXene Composites for Efficient Photocatalytic Degradation of Congo Red Dye. *ACS Omega* **2019**, *4*, 8661–8668. [CrossRef] [PubMed]

13. Bharathkumar, S.; Sakar, M.; Balakumar, S. Experimental Evidence for the Carrier Transportation Enhanced Visible Light Driven Photocatalytic Process in Bismuth Ferrite (BiFeO$_3$) One-Dimensional Fiber Nanostructures. *J. Phys. Chem. C* **2016**, *120*, 18811–18821. [CrossRef]

14. Tang, J.; Wang, R.; Liu, M.; Zhang, Z.; Song, Y.; Xue, S.; Zhao, Z.; Dionysiou, D.D. Construction of novel Z-scheme Ag/FeTiO$_3$/Ag/BiFeO$_3$ photocatalyst with enhanced visible-light-driven photocatalytic performance for degradation of norfloxacin. *Chem. Eng. J.* **2018**, *351*, 1056–1066. [CrossRef]

15. Niloy, N.R.; Chowdhury, M.I.; Shanto, M.A.H.; Islam, J.; Rhaman, M.M. Multiferroic Bismuth ferrite nanocomposites as a potential photovoltaic material. *IOP Conf. Ser. Mater. Sci. Eng.* **2021**, *1091*, 012049. [CrossRef]

16. Park, B.-G. Bismuth ferrite thin film coated on polycarbonate surface and its photocatalytic properties in visible light. *Mater. Lett.* **2021**, *285*, 129006. [CrossRef]

17. Saravanakumar, K.; Park, C.M. Rational design of a novel LaFeO$_3$/g-C$_3$N$_4$/BiFeO$_3$ double Z-scheme structure: Photocatalytic performance for antibiotic degradation and mechanistic insight. *Chem. Eng. J.* **2021**, *423*, 130076. [CrossRef]

18. Mostafaloo, R.; Mahmoudian, M.H.; Asadi-Ghalhari, M. BiFeO$_3$/Magnetic nanocomposites for the photocatalytic degradation of cefixime from aqueous solutions under visible light. *J. Photochem. Photobiol. A Chem.* **2019**, *382*, 111926. [CrossRef]

19. Balta, Z.; Simsek, E.B. Uncovering the systematical charge separation effect of boron nitride quantum dots on photocatalytic performance of BiFeO$_3$ perovskite towards degradation of tetracycline antibiotic. *J. Environ. Chem. Eng.* **2021**, *9*, 106567. [CrossRef]

20. Jiang, Y.; Xing, C.; Chen, Y.; Shi, J.; Wang, S. Preparation of BiFeO$_3$ and photodegradation of tetracycline pollutant in the UV-heterogeneous Fenton-like system. *Environ. Sci. Pollut. Res.* **2022**, *29*, 57656–57668. [CrossRef]

21. Imessaoudene, A.; Cheikh, S.; Bollinger, J.-C.; Belkhiri, L.; Tiri, A.; Bouzaza, A.; El Jery, A.; Assadi, A.; Amrane, A.; Mouni, L. Zeolite Waste Characterization and Use as Low-Cost, Ecofriendly, and Sustainable Material for Malachite Green and Methylene Blue Dyes Removal: Box-Behnken Design, Kinetics, and Thermodynamics. *Appl. Sci.* **2022**, *12*, 7587. [CrossRef]

22. Chedri Mammar, A.; Mouni, L.; Bollinger, J.-C.; Belkhiri, L.; Bouzaza, A.; Assadi, A.A.; Belkacemi, H. Modeling and optimization of process parameters in elucidating the adsorption mechanism of Gallic acid on activated carbon prepared from date stones. *Sep. Sci. Technol.* **2020**, *55*, 3113–3125. [CrossRef]

23. Bouchelkia, N.; Mouni, L.; Belkhiri, L.; Bouzaza, A.; Bollinger, J.-C.; Madani, K.; Dahmoune, F. Removal of lead(II) from water using activated carbon developed from jujube stones, a low-cost sorbent. *Sep. Sci. Technol.* **2016**, *51*, 1645–1653. [CrossRef]

24. Zhang, M.; Song, G.; Gelardi, D.L.; Huang, L.; Khan, E.; Mašek, O.; Parikh, S.J.; Ok, Y.S. Evaluating biochar and its modifications for the removal of ammonium, nitrate, and phosphate in water. *Water Res.* **2020**, *186*, 116303. [CrossRef]

25. Huang, Q.; Chen, C.; Zhao, X.; Bu, X.; Liao, X.; Fan, H.; Gao, W.; Hu, H.; Zhang, Y.; Huang, Z. Malachite green degradation by persulfate activation with CuFe$_2$O$_4$@biochar composite: Efficiency, stability and mechanism. *J. Environ. Chem. Eng.* **2021**, *9*, 105800. [CrossRef]

26. Yi, Y.; Luo, J.; Fang, Z. Magnetic biochar derived from Eichhornia crassipes for highly efficient Fenton-like degradation of antibiotics: Mechanism and contributions. *J. Environ. Chem. Eng.* **2021**, *9*, 106258. [CrossRef]

27. Roy, A.; Chakraborty, S.; Kundu, S.P.; Adhikari, B.; Majumder, S.B. Adsorption of Anionic-Azo Dye from Aqueous Solution by Lignocellulose-Biomass Jute Fiber: Equilibrium, Kinetics, and Thermodynamics Study. *Ind. Eng. Chem. Res.* **2012**, *51*, 12095–12106. [CrossRef]

28. Saeed, A.; Harun, N.; Sufian, S.; Afolabi, H.; Al-Qadami, E.; Roslan, F.; Rahim, S.; Ghaleb, A. Production and Characterization of Rice Husk Biochar and Kenaf Biochar for Value-Added Biochar Replacement for Potential Materials Adsorption. *Ecol. Eng. Environ. Technol.* **2021**, *22*, 1–8. [CrossRef]

29. Park, H.; Byun, J.; Han, J. Economically feasible thermochemical process for methanol production from kenaf. *Energy* **2021**, *230*, 120729. [CrossRef]

30. Yang, H.; Ye, S.; Zeng, Z.; Zeng, G.; Tan, X.; Xiao, R.; Wang, J.; Song, B.; Du, L.; Qin, M.; et al. Utilization of biochar for resource recovery from water: A review. *Chem. Eng. J.* **2020**, *397*, 125502. [CrossRef]

31. Haromae, H.; Pattananuwat, P. Preparation of bismuth ferrite as photo-supercapacitive electrode. *IOP Conf. Ser. Mater. Sci. Eng.* **2019**, *600*, 012005. [CrossRef]

32. Odinga, E.S.; Waigi, M.G.; Gudda, F.O.; Wang, J.; Yang, B.; Hu, X.; Li, S.; Gao, Y. Occurrence, formation, environmental fate and risks of environmentally persistent free radicals in biochars. *Environ. Int.* **2020**, *134*, 105172. [CrossRef] [PubMed]

33. Xue, K.-H.; Wang, J.; Yan, Y.; Peng, Y.; Wang, W.-L.; Xiao, H.-B.; Wang, C.-C. Enhanced As(III) transformation and removal with biochar/SnS$_2$/phosphotungstic acid composites: Synergic effect of overcoming the electronic inertness of biochar and W$_2$O$_3$(AsO$_4$)$_2$ (As(V)-POMs) coprecipitation. *J. Hazard. Mater.* **2021**, *408*, 124961. [CrossRef] [PubMed]

34. Yu, F.; Tian, F.; Zou, H.; Ye, Z.; Peng, C.; Huang, J.; Zheng, Y.; Zhang, Y.; Yang, Y.; Wei, X.; et al. ZnO/biochar nanocomposites via solvent free ball milling for enhanced adsorption and photocatalytic degradation of methylene blue. *J. Hazard. Mater.* **2021**, *415*, 125511. [CrossRef] [PubMed]

35. Mushtaq, F.; Chen, X.; Hoop, M.; Torlakcik, H.; Pellicer, E.; Sort, J.; Gattinoni, C.; Nelson, B.J.; Pané, S. Piezoelectrically Enhanced Photocatalysis with BiFeO$_3$ Nanostructures for Efficient Water Remediation. *iScience* **2018**, *4*, 236–246. [CrossRef]

36. Alikhanov, N.M.R.; Rabadanov, M.K.; Orudzhev, F.F.; Gadzhimagomedov, S.K.; Emirov, R.M.; Sadykov, S.A.; Kallaev, S.N.; Ramazanov, S.M.; Abdulvakhidov, K.G.; Sobola, D. Size-dependent structural parameters, optical, and magnetic properties of facile synthesized pure-phase $BiFeO_3$. *J. Mater. Sci. Mater. Electron.* **2021**, *32*, 13323–13335. [CrossRef]

37. Cai, X.; Li, J.; Liu, Y.; Hu, X.; Tan, X.; Liu, S.; Wang, H.; Gu, Y.; Luo, L. Design and Preparation of Chitosan-Crosslinked Bismuth Ferrite/Biochar Coupled Magnetic Material for Methylene Blue Removal. *Int. J. Environ. Res. Public Health* **2019**, *17*, 6. [CrossRef]

38. Li, S.; Wang, P.; Zheng, H.; Zheng, Y.; Zhang, G. Adsorption and one-step degradation-regeneration of 4-amino-5-hydroxynaphthalene-2,7-disulfonic acid using biochar-based $BiFeO_3$ nanocomposites. *Bioresour. Technol.* **2017**, *245*, 1103–1109. [CrossRef]

39. Zhou, D.; Xie, G.; Hu, X.; Cai, X.; Zhao, Y.; Hu, X.; Jin, Q.; Fu, X.; Tan, X.; Liang, C.; et al. Coupling of kenaf Biochar and Magnetic $BiFeO_3$ onto Cross-Linked Chitosan for Enhancing Separation Performance and Cr(VI) Ions Removal Efficiency. *Int. J. Environ. Res. Public Health* **2020**, *17*, 788. [CrossRef]

40. Liu, N.; Hu, Z.; Hao, L.; Bai, H.; He, P.; Niu, R.; Gong, J. Trash into treasure: Converting waste polyester into C_3N_4-based intramolecular donor-acceptor conjugated copolymer for efficient visible-light photocatalysis. *J. Environ. Chem. Eng.* **2022**, *10*, 106959. [CrossRef]

41. Zhao, N.; Li, B.; Huang, H.; Lv, X.; Zhang, M.; Cao, L. Modification of kelp and sludge biochar by TMT-102 and NaOH for cadmium adsorption. *J. Taiwan Inst. Chem. Eng.* **2020**, *116*, 101–111. [CrossRef]

42. Hou, L.; Li, X.; Yang, Q.; Chen, F.; Wang, S.; Ma, Y.; Wu, Y.; Zhu, X.; Huang, X.; Wang, D. Heterogeneous activation of peroxymonosulfate using Mn-Fe layered double hydroxide: Performance and mechanism for organic pollutant degradation. *Sci. Total Environ.* **2019**, *663*, 453–464. [CrossRef] [PubMed]

43. Xie, X.; Xiong, H.; Zhang, Y.; Tong, Z.; Liao, A.; Qin, Z. Preparation magnetic cassava residue microspheres and its application for Cu(II) adsorption. *J. Environ. Chem. Eng.* **2017**, *5*, 2800–2806. [CrossRef]

44. Zheng, X.; Wang, J.; Liu, J.; Wang, Z.; Chen, S.; Fu, X. Photocatalytic degradation of benzene over different morphology $BiPO_4$: Revealing the significant contribution of high–energy facets and oxygen vacancies. *Appl. Catal. B Environ.* **2019**, *243*, 780–789. [CrossRef]

45. Gao, M.Y.; Chen, X.W.; Huang, W.X.; Wu, L.; Yu, Z.S.; Xiang, L.; Mo, C.H.; Li, Y.W.; Cai, Q.Y.; Wong, M.H.; et al. Cell wall modification induced by an arbuscular mycorrhizal fungus enhanced cadmium fixation in rice root. *J. Hazard. Mater.* **2021**, *416*, 125894. [CrossRef]

46. Jadhav, V.V.; Zate, M.K.; Liu, S.; Naushad, M.; Mane, R.S.; Hui, K.N.; Han, S.-H. Mixed-phase bismuth ferrite nanoflake electrodes for supercapacitor application. *Appl. Nanosci.* **2015**, *6*, 511–519. [CrossRef]

47. Zhao, L.; Guo, L.; Tang, Y.; Zhou, J.; Shi, B. Novel g-C_3N_4/C/Fe_2O_3 Composite for Efficient Photocatalytic Reduction of Aqueous Cr(VI) under Light Irradiation. *Ind. Eng. Chem. Res.* **2021**, *60*, 13594–13603. [CrossRef]

48. Hu, X.; Wang, W.; Xie, G.; Wang, H.; Tan, X.; Jin, Q.; Zhou, D.; Zhao, Y. Ternary assembly of g-C_3N_4/graphene oxide sheets /$BiFeO_3$ heterojunction with enhanced photoreduction of Cr(VI) under visible-light irradiation. *Chemosphere* **2019**, *216*, 733–741. [CrossRef]

49. Zhu, H.; Chen, T.; Liu, J.; Li, D. Adsorption of tetracycline antibiotics from an aqueous solution onto graphene oxide/calcium alginate composite fibers. *RSC Adv.* **2018**, *8*, 2616–2621. [CrossRef]

50. Wu, C.; Zhang, J.; Fang, B.; Cui, Y.; Xing, Z.; Li, Z.; Zhou, W. Self-floating biomass charcoal supported flower-like plasmon silver/carbon, nitrogen co-doped defective TiO_2 as robust visible light photocatalysts. *J. Clean. Prod.* **2021**, *329*, 129723. [CrossRef]

51. Xu, R.; Li, M.; Zhang, Q. Collaborative optimization for the performance of ZnO/biochar composites on persulfate activation through plant enrichment-pyrolysis method. *Chem. Eng. J.* **2022**, *429*, 132294. [CrossRef]

52. Ruan, X.; Sun, Y.; Du, W.; Tang, Y.; Liu, Q.; Zhang, Z.; Doherty, W.; Frost, R.L.; Qian, G.; Tsang, D.C.W. Formation, characteristics, and applications of environmentally persistent free radicals in biochars: A review. *Bioresour. Technol.* **2019**, *281*, 457–468. [CrossRef] [PubMed]

53. Kumar, A.; Sharma, S.K.; Sharma, G.; Al-Muhtaseb, A.A.H.; Naushad, M.; Ghfar, A.A.; Stadler, F.J. Wide spectral degradation of Norfloxacin by Ag@$BiPO_4$/BiOBr/$BiFeO_3$ nano-assembly: Elucidating the photocatalytic mechanism under different light sources. *J. Hazard. Mater.* **2019**, *364*, 429–440. [CrossRef] [PubMed]

54. Cao, T.-T.; Cui, H.; Zhang, Q.-W.; Cui, C.-W. Facile synthesis of Co(II)-BiOCl@biochar nanosheets for photocatalytic degradation of p-nitrophenol under vacuum ultraviolet (VUV) irradiation. *Appl. Surf. Sci.* **2021**, *559*, 149938. [CrossRef]

55. Wang, T.; Bai, Y.; Si, W.; Mao, W.; Gao, Y.; Liu, S. Heterogeneous photo-Fenton system of novel ternary Bi_2WO_6/$BiFeO_3$/g-C_3N_4 heterojunctions for highly efficient degrading persistent organic pollutants in wastewater. *J. Photochem. Photobiol. A Chem.* **2021**, *404*, 112856. [CrossRef]

56. Gao, F.; Chen, X.Y.; Yin, K.B.; Dong, S.; Ren, Z.F.; Yuan, F.; Yu, T.; Zou, Z.; Liu, J.M. Visible-light photocatalytic properties of weak magnetic $BiFeO_3$ nanoparticles. *Adv. Mater.* **2007**, *19*, 2889. [CrossRef]

57. Kumar, A.; Kumar, A.; Sharma, G.; Naushad, M.; Stadler, F.J.; Ghfar, A.A.; Dhiman, P.; Saini, R.V. Sustainable nano-hybrids of magnetic biochar supported g-C_3N_4/$FeVO_4$ for solar powered degradation of noxious pollutants- Synergism of adsorption, photocatalysis & photo-ozonation. *J. Clean. Prod.* **2017**, *165*, 431–451. [CrossRef]

58. Yang, H.; Yu, H.; Wang, J.; Ning, T.; Chen, P.; Yu, J.; Di, S.; Zhu, S. Magnetic porous biochar as a renewable and highly effective adsorbent for the removal of tetracycline hydrochloride in water. *Environ. Sci. Pollut. Res.* **2021**, *28*, 61513–61525. [CrossRef]